Acta Pharmaceutica Sinica B 2026;16(2):966−978

Chinese Pharmaceutical Association
Institute of Materia Medica, Chinese Academy of Medical Sciences

Acta Pharmaceutica Sinica B

www.elsevier.com/locate/apsb
www.sciencedirect.com

ORIGINAL ARTICLE

Complete biosynthesis of phenylspirodrimanes with unclustered genes in *Stachybotrys chartarum*

Jimei Liu, Ridao Chen, Min Zhang, Yangyang Duan, Keping Feng, Songyang Sui, Yaotian Han, Kebo Xie, Jun Wu, Haibo Yu, Dawei Chen*, Jungui Dai*

State Key Laboratory of Bioactive Substance and Function of Natural Medicines, NHC Key Laboratory of Biosynthesis of Natural Products, CAMS Key Laboratory of Enzyme and Biocatalysis of Natural Drugs, and Beijing Key Laboratory of Non-Clinical Drug Metabolism and PK/PD Study, Institute of Materia Medica, Chinese Academy of Medical Sciences and Peking Union Medical College, Beijing 100050, China

Received 18 April 2025; received in revised form 20 May 2025; accepted 9 June 2025

KEY WORDS

Biosynthesis;
Phenylspirodrimane;
Unclustered genes;
Hierarchical clustering analysis;
Expression correlation analysis;
Stachybotrys chartarum;
Meroterpenoid;
Multiple gene clusters

Abstract Phenylspirodrimanes are a class of structurally diverse meroterpenoids, including the bioactive dimer stachybocin A (**1**) and the high-reactivity monomer stachybotrydial (**2**), which are isolated from the genus *Stachybotrys*. Whereas the biosynthetic pathway of these phenylspirodrimane meroterpenoids has remained elusive. Herein, we deciphered the complete biosynthetic pathway of **2** with unprecedented two gene clusters and five discrete genes by genome mining, gene inactivation, heterologous expression, biochemical experiments, and especially combining with transcriptome-based hierarchical clustering and expression correlation analyses. Totally, 11 genes for the phenylspirodrimane core skeleton formation, 8′-methyl oxidation, and 3-OH epimerization were efficiently discovered and functionally characterized. Notably, these biosynthetic genes are distributed across seven distinct regions, with a rare combination of multiple gene clusters and genes outside the clusters. Bioactivity assays revealed that four intermediates **6**−**8**, and **9a** exhibited significant inhibitory effect on the inactivated state $hNa_V1.2$ channels with IC_{50} values of 0.15, 0.04, 0.28, and 1.91 μmol/L, respectively. These findings expand our understanding of phenylspirodrimane-type meroterpenoid biosynthesis and underscore the utility of transcriptome-based hierarchical clustering and expression correlation analyses for identifying unclustered biosynthetic genes in fungi.

*Corresponding authors.
E-mail addresses: chendawei@imm.ac.cn (Dawei Chen), jgdai@imm.ac.cn (Jungui Dai).

Peer review under the responsibility of Chinese Pharmaceutical Association and Institute of Materia Medica, Chinese Academy of Medical Sciences.

https://doi.org/10.1016/j.apsb.2025.09.015

1. Introduction

Meroterpenoids are a diverse family of hybrid natural products, consisting of a terpenoid and a non-terpenoid portion[1-4]. Most of fungal meroterpenoids possess a polyketide-derived portion as their nonterpenoid moiety[1,2]. Representative fungal meroterpenoids with a polyketide substructure are derived from 3,5-dimethylorsellinic acid (DMOA) and orsellinic acid (OA). Among them, the DMOA-derived compounds are the most abundant and structurally diverse[1-4], and their biosynthetic pathways have been well studied[5-11]. Meroterpenoids derived from OA were discovered and isolated several decades ago, including LL-Z1272β[12], ascochlorin[13], ascofuranone[14], SMTPs[15], kampanols[15], bisabosquals[15], and phenylspirodrimanes[15]. To date, the biosynthetic pathways of only a few compounds, such as LL-Z1272β[16], ascochlorin[17], and ascofuranone[17], have been elucidated, while most of the OA-derived meroterpenoids remain largely enigmatic.

Phenylspirodrimanes are a class of structurally complex and diverse meroterpenoids derived from OA, which consist of a common drimane-type sesquiterpene skeleton with a benzene ring fused through a spirofuran (Fig. 1). More than 150 compounds, including monomers and dimers, have been identified from the genus *Stachybotrys* since K-76, the first compound, was isolated in 1979[18]. These compounds display a broad spectrum of biological activities[15,19-27], including endothelin receptor antagonism, anticomplement, antiviral, antibacterial, anti-inflammatory, protein tyrosine phosphatase 1B (PTP1B) inhibitory, *N*-methyl-D-aspartate (NMDA) receptor antagonistic, and cytotoxic activities. In our previous work, we isolated numerous phenylspirodrimane monomers and diverse structural scaffold dimers from *S. chartarum* CGMCC 3.5365[23-26], including novel dimers with a 6/7 oxygen heterocycle, cyclopentanone, [5,6]-spiroketal, and furan/furan linkages (Fig. 1). Among these compounds, the dimer stachybocin A (**1**) (Fig. 1) can significantly inhibit the inactivation of the $hNa_V1.2$ channels, indicating that it is a promising lead compound for the treatment of epilepsy[27]. Furthermore, it has been reported that stachybocin A (**1**) could be synthesized *via* the non-enzymatic reaction between the highly reactive monomer stachybotrydial (**2**) with an *O*-phthalaldehyde unit (Fig. 1) and L-lysine[27]. More important, diversified phenylspirodrimane lactones, lactams, and dimers could also be generated *via* the enzymatic/non-enzymatic reactions from **2**[15,24-27], indicating the great potential of **2** for the use as a starting material in diversity-oriented synthesis.

The structural complexity and remarkable bioactivities of phenylspirodrimane meroterpenoids have attracted increasing attention in their isolation, structure elucidation, chemical synthesis, and bioactivity characterization[15,18-29], however, their biosynthesis has not yet been elucidated. In 2016, Abe and coworkers identified the genes involved in the synthesis of LL-Z1272β (**4**)[16], a well-known precursor of many meroterpenoids[17,30], which originates from OA (**5**) and farnesyl diphosphate (FPP). By comparing the structures of **2** and **4**, we speculated that the biosynthesis of **2** may follow a pathway similar to that of **4** in the early stages. Whereas the complete biosynthetic process of **2**, particularly the genes/enzymes responsible for cyclization and post-modification reactions, remains unclear. Therefore, elucidating the long-standing biosynthesis of **2** would provide a comprehensive understanding of the phenylspirodrimane meroterpenoid biosynthetic process and present an opportunity for engineering microorganisms to produce bioactive dimer **1** and other derivatives for drug discovery.

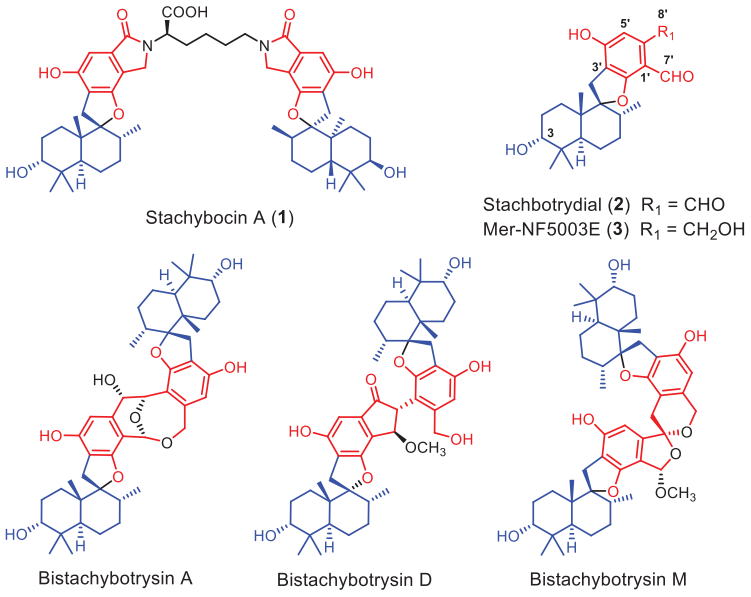

Figure 1 Representative phenylspirodrimanes from *S. chartarum*. Polyketide moieties are shown in red and terpenoid moieties are shown in blue.

Generally, current approaches for deciphering fungal natural product biosynthetic pathways rely heavily on the genomic clustering of biosynthetic genes[31,32]. This feature can be predicted by screening the genome for collocated genes with functional motifs for putative biosynthetic enzymes[33], however, unclustered gene candidates are frequently overlooked and remain difficult to discover and functionally characterize. Recently, multiple gene clusters and unclustered examples have been reported in fungi, where differential transcriptome analysis[17,34], homology-based approach[7,35], and phylogenetic study[36] were employed to identify these exceptional biosynthetic genes. Whereas there is still no established strategy to explore multilocus and unknown biosynthetic genes in fungi. As the biosynthetic genes for plant metabolites are often unclustered, co-expression and hierarchical clustering analyses have typically been employed to mine and identify such unclustered biosynthetic genes[37-39]. Accordingly, this strategy might be useful for discovering the biosynthetically unclustered genes responsible for fungal metabolites.

Herein, we first identified the unclustered biosynthetic genes for **2** in *S. chartarum* by employing combinatorial strategies including genome mining, gene inactivation, heterologous expression, biochemical experiments, and particularly the transcriptome-based hierarchical clustering and expression correlation analyses. Consequently, 11 functional genes are efficiently discovered and functionally characterized. Interestingly, these biosynthetic genes for **2** are not under the control of well-defined gene cluster, but scattered across seven distinct regions in the genome (Fig. 2A). Moreover, the biosynthetic pathways of these phenylspirodrimane meroterpenoids were consisted with a complex network. Bioassays revealed that four intermediates **6**–**8**, and **9a** exhibited significant $hNa_V1.2$ channels inhibitory activity.

2. Results and discussion

*2.1. The sta-1 cluster genes are responsible for the biosynthesis of LL-Z1272β (**4**)*

To explore the biosynthetic gene clusters (BGCs) of **2**, whole genome sequencing was performed on *S. chartarum* CGMCC 3.5365, yielding 37.5 Mb of genomic data. According to the

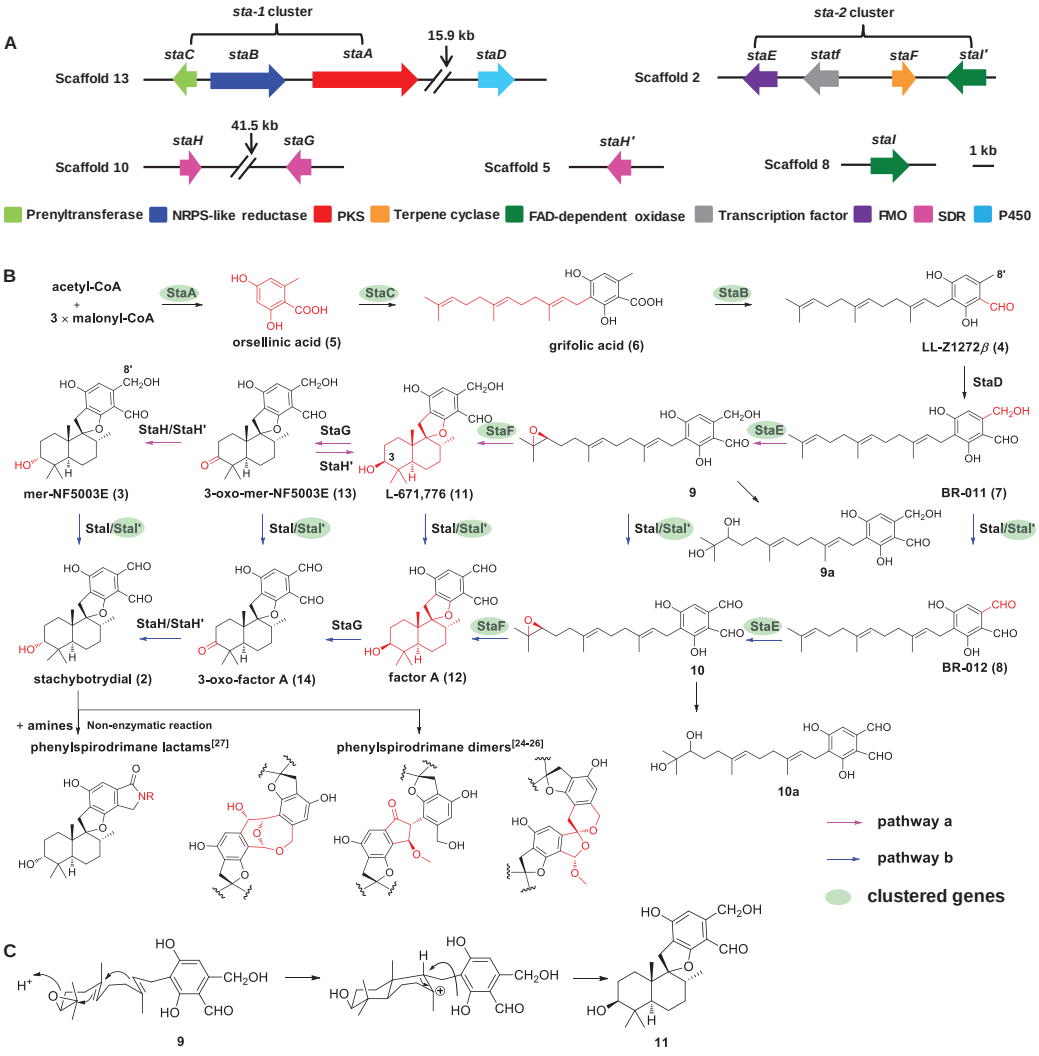

Figure 2 The proposed biosynthetic pathway of phenylspirodrimanes in *S. chartarum*. (A) Schematic representation of the genes involved in the biosynthesis of **2**. (B) The overall scheme of the proposed biosynthesis of phenylspirodrimanes. (C) The cyclization reaction catalyzed by StaF.

reported biosynthetic pathways of meroterpenoids[2-4], the genes responsible for the formation of the basic skeleton of **2** may include the polyketide synthase (PKS) and prenyltransferase (PT) genes. Therefore, a candidate biosynthesis-related gene cluster, *sta-1*, comprising three genes—a nonreducing PKS gene *staA*, a UbiA-like PT gene *staC*, and an NRPS-like reductase gene *staB*—was selected from the genome (Fig. 2A). The amino acid sequences of *staA*−*C* were 75.3%, 74.8%, and 75.5% identical to those of *stbA*−*C* (the genes responsible for the biosynthesis of **4** in *S. bisbyi*)[16] (Supporting Information Table S1), suggesting that *sta*-1 might be responsible for the biosynthesis of **2**. By heterologously expressing *staA*−*C* in *Aspergillus oryzae* NSAR1[40] and analyzing the metabolites that accumulated in the mycelia of the transformants by HPLC, **4** was detected in the strain harboring *staA*−*C*, as confirmed by comparison with an authentic standard and NMR data (Supporting Information Fig. S1 and Table S2). Moreover, we obtained Δ*staC* and Δ*staB* strains (Supporting Information Fig. S2). LC−MS analyses of the metabolites from these two strains revealed that neither of the two knockout strains yielded **2** (Fig. S1), while accumulation of the corresponding intermediates orsellinic acid (**5**) and grifolic acid (**6**) was observed, respectively (Fig. S1 and Supporting Information Table S2). In addition, the coding sequence of *staC* was cloned and inserted into pESC-His and expressed in *Saccharomyces cerevisiae* INVSc1, and microsomal StaC was incubated with **5** in the presence of FPP and Mg^{2+}. Conversion of **5** to **6** was clearly detected (Supporting Information Fig. S3). Therefore, *sta-1* cluster genes (*staA*−*C*) have been characterized to be involved in the biosynthesis of **2** for the formation of its precursor **4**.

2.2. *Sta-2 cluster genes catalyze phenylspirodrimane core skeleton formation*

Typically, the biosynthesis of most fungal meroterpenoids undergo epoxidation of the prenyl terminal double bond by a flavin-dependent monooxygenase (FMO) and subsequent cyclization of the epoxide by a membrane-bound terpene cyclase (TPC), followed by various tailoring reactions (*e.g.*, oxidation and reduction)[2-4]. Accordingly, we conducted a comprehensive scan of the genes flanking *staA*−*C* to identify potential additional biosynthetic genes and deleted 7 genes, including FMOs, annotated membrane-bound proteins, and oxidase genes (Supporting Information Fig. S4). Upon cultivation of these knockout strains and metabolite analysis, the production of **2** was detected in all the mutant strains, suggesting that additional biosynthetic genes are located outside of the *sta-1* cluster.

Therefore, we sought to identify potential terpene cyclase genes involved in the biosynthesis of **2** through a comprehensive genome-wide sequence homology-based search. A local BLAST search of the *S. chartarum* genome was performed using the amino acid sequences of the known meroterpenoid cyclases Pyr4[40] and MacJ[41] as queries to identify candidate terpene cyclases for **2** (Supporting Information Fig. S5). Pyr4 serves as a model meroterpenoid cyclase involved in the biosynthesis of pyripyropene A[40], while MacJ is naturally involved in the biosynthetic pathway of the drimane-type meroterpenoid macrophorin A[41]. This analysis led to the identification of orthologs two candidate genes, A00874 and A04827 (Fig. S5), sharing 25%−30% amino acid identities to Pyr4 and MacJ. Subsequently, gene-deleted strains were generated (Fig. S2), and further analysis of their metabolites revealed that the production of **2** was completely abolished in Δ*A04827* (Δ*staF*) (Fig. 3A, ii), while the A00874 mutant (Δ*A00874*) still retained the ability to produce **2** (Supporting Information Fig. S6, ii). Therefore, A04827 has been identified as a terpene cyclase gene involved in the biosynthesis of **2** and is designated as *staF*.

Moreover, the A04825 gene (*staE*) located in the flanking region of *staF* was annotated as an FMO gene (Fig. 2A), suggesting its potential involvement in the biosynthesis of **2** for epoxidation of the end double bond of the farnesyl moiety, as in pyripyropene A[40] biosynthesis. Consequently, a Δ*staE* mutant was created (Fig. S2), which lost the ability to generate **2** (Fig. 3A, iii), however, no intermediate accumulated in the Δ*staE* strain under the same fermentation conditions as in wild-type strain cultivated for 7 days in PDB media (Fig. 3A, i and iii). Therefore, the metabolite profile of this mutant was time-course monitored, and initial production of **7** followed by the formation of oxidized product **8** (Fig. 3B) was observed by using LC−MS analyses. The structures of **7** and **8** were identified as BR-011 and BR-012, respectively, based on MS and NMR analyses (Supporting Information Table S3 and Fig. S7; and Fig. 2B). Moreover, the restoration of **2** production in the Δ*staB* mutant upon individual feeding with **7** or **8** supported these compounds as biosynthetic intermediates (Supporting Information Fig. S8). In addition, cultivation of the Δ*staF* mutant (Fig. 3A, ii) led to the production of two major metabolites (**9a** and **10a**), whose structures were characterized as the dihydroxylated derivatives of **7** and **8**, respectively, by NMR and MS analyses (Supporting Information Table S4 and Fig. S7). These observations suggested that **7** and **8** were epoxidized into **9** and **10** by StaE, respectively (Fig. 2B), and thereafter **9** and **10** were transformed into the corresponding diol products **9a** and **10a** non-enzymatically or through endogenous hydrolase in *S. chartarum*.

With compounds **7** and **8** in hand, an *in vitro* biochemical assay was conducted to confirm the function of StaE. The coding sequence of *staE* was cloned and inserted into pCold-TF expression vector, resulting in robust expression in *Escherichia coli* Transetta (DE3) (Supporting Information Fig. S9). Incubation of StaE with FAD, NADPH, and **7** led to the formation of **9** (Fig. 3C). The purification of **9** from a large-scale enzymatic reaction was very difficult due to its inherent structural instability. In contrast, **9a**, a non-enzymatic derivative of **9** that possesses a farnesyl chain with a diol at the C-10 and C-11 positions, was isolated from this reaction (Supporting Information Fig. S10). Subsequently, we attempted to biochemically elucidate the activity of StaE toward **8**. Incubation of StaE with **8** resulted in the complete disappearance of **8** without any new peaks in both the experimental and control groups (Supporting Information Fig. S11). This observation might be attributed to the reactive *O*-phthalaldehyde unit in **8**, which can react nonspecifically with the free amine groups of the protein[27,42]. Overall, StaE, an FMO, has been characterized to be responsible for the epoxidation of the end double bond of the farnesyl moiety in the biosynthesis of **2**.

Since StaF is a membrane-bound protein, the coding region of *staF* was cloned and inserted into the pESC-His expression vector, and the recombinant plasmid was subsequently transformed into *S. cerevisiae* for microsomal preparation. When StaE and StaF were combined and incubated with **7** (Fig. 3D), a new product, **11**, was detected by HPLC−MS. Notably, **11** exhibited a molecular weight and UV absorption spectrum identical to those of **3** but showed significantly different HPLC retention times (**11** at 18.2 min *vs.* **3** at 21.9 min; Fig. 3D and Fig. S7), suggesting that **11** could be an isomer of **3**. After scale-up incubation, **11** was obtained and subjected to NMR analyses, revealing that the only

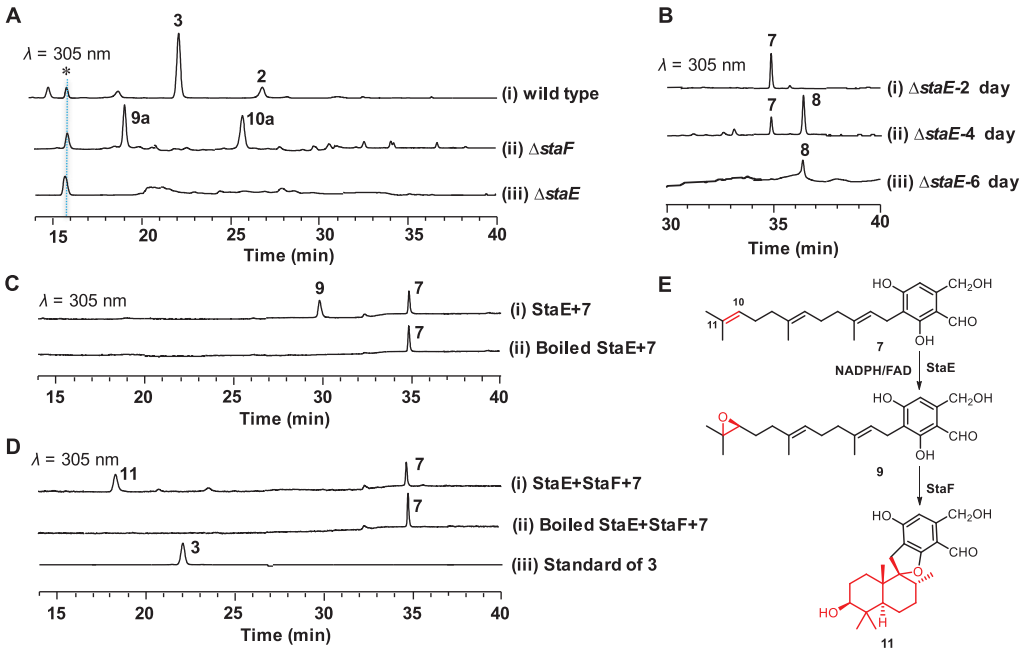

Figure 3 Functional characterizations of StaE and StaF. (A) HPLC analysis of metabolites from wild-type *S. chartarum* and mutants: (i) wild-type; (ii) Δ*staF* strain; (iii) Δ*staE* strain. (B) Time course of metabolites for the Δ*staE* strain: (i) 2-day-old cultures; (ii) 4-day-old cultures; (iii) 6-day-old cultures. (C) HPLC analysis of *in vitro* enzymatic reactions with StaE: (i) **7**; (ii) **7** with inactivated StaE. (D) HPLC analysis of *in vitro* enzymatic reactions with StaE and StaF: (i) **7**; (ii) **7** with inactivated StaE and StaF; (iii) authentic **3**. (E) Schematic representation of the oxidation and cyclization of **7** by StaE and StaF, respectively. The asterisk (*) denotes the unrelated metabolite mellein.

difference between **11** and **3** was the configuration of 3-OH (Supporting Information Table S5). The *β*-OH configuration in **11** was confirmed by the coupling pattern of H-3 in ^{1}H NMR (dd, J = 10.5 and 5.4 Hz in **11** *vs.* brs in **3**) and the chemical shift of C-3 (76.5 in **11** *vs.* 73.4 in **3**). Thus, compound **11** was identified as L-671,776 (also known as factor B)[43,44], which has the basic skeleton of phenylspirodrimane. These results supported that StaF is the TPC involved in the biosynthesis of **2**, catalyzing the terpene cyclization to yield **11** (Fig. 3E). Subsequently, *A. oryzae* transformants harboring *staE* and *staEF* were individually constructed. Feeding compound **7** to the *A. oryzae-staE* and *A. oryzae-staEF* strains resulted in the production of **9a** and **11**, respectively (Supporting Information Fig. S12), which further confirmed the above deduction. Recently, another TPC MfmH involved in the biosynthesis of drimane-type meroterpenoid has been reported[45], which shares 31% and 54% amino acid identity to StaF and MacJ, respectively. Both MfmH and MacJ can directly protonate an olefinic double bond, whereas StaF accepts an epoxide as a substrate and catalyzes the cyclization (Fig. 2C).

2.3. Cytochrome P450 monooxygenase staD catalyzes 8′-hydroxylation

According to the above results, it can be concluded that StaA−C catalyze the biosynthesis of **4**, StaE epoxidizes the terminal olefin of **7** to produce **9**, and subsequently StaF cyclizes **9** into **11** in the biosynthetic pathway of **2** (Fig. 2B and C). Then, a postulated enzyme for oxidizing the C-8′ methyl group of **4** into a hydroxymethyl to give **7** is necessary. Subsequently, we sought to identify the requisite oxidase genes involved in the biosynthesis of **2** and deleted 11 oxidase genes adjacent to *staE* and *staF* (Fig. S4). All these deletion strains retained the ability to produce **2**, suggesting that the responsible oxidase gene is outside of the two gene clusters (*sta-1* and *sta-2*) and located elsewhere in the genome.

To identify the enzymes responsible for oxidizing the 8′-methyl group in **4**, we first focused on cytochrome P450 monooxygenases, which might catalyze methyl oxidation[46]. As mentioned above, the corresponding genes were not clustered with the *sta-1* and *sta-2* clusters, presenting a great challenge for the identification of candidate genes due to large number of P450 monooxygenase genes (∼150) in the *S. chartarum* genome and the very limited availability of relevant gene information. Therefore, a comprehensive analysis of the accumulation of **2** and **3** (the predominant phenylspirodrimane secondary metabolites) in *S. chartarum* cultures under various cultivated conditions was conducted. Interestingly, significant variations were observed in the levels of these compounds across different culture times and media. The greatest accumulations of both compounds were found in 4-day-old samples in PDB media, while only trace amounts were detected in 2-day-old samples in DPY media (Supporting Information Fig. S13). Thereafter, we conducted a comparative transcriptome analysis on *S. chartarum* samples with varying levels of **2** and **3** accumulation (mycelia from PDB media cultured for 2 and 4 days, as well as mycelia from DPY media cultured for 2 days). Based on a hierarchical clustering analysis of all CYP450 genes from *S. chartarum*, 13 genes were found to exhibit similar transcript expression profiles to those of *staA−C*, E, and F (Fig. 4A). Furthermore, 6 out of these 13 genes showed high expression correlation with previously identified genes ($r > 0.6$ with each gene, Pearson correlation coefficient) (Supporting Information Table S6). Subsequently, these 6 genes were prioritized

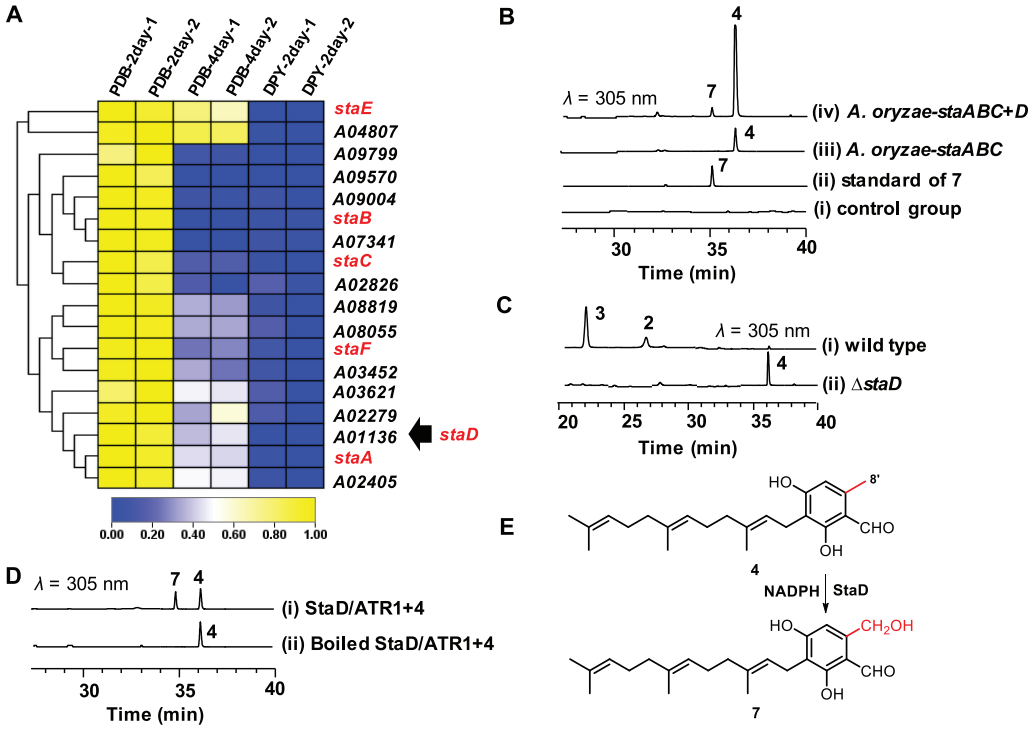

Figure 4 Mining and characterization of StaD for the hydroxylation of 8′-methyl in the biosynthesis of **2**. (A) Hierarchical clustering of expression analysis for candidate CYP450 genes. The heatmap depicts the expression levels from a single node from the resulting cluster. Color key: identified genes (red), candidate CYP450 genes (black), and gene (*staD*) identified in this part (black arrow). Samples from the mycelia of *S. chartarum* cultured in distinct media and for different durations (PDB media cultured for 2 and 4 days, as well as DPY media cultured for 2 days). (B) HPLC analysis of the metabolites of engineered *A. oryzae* transformants: (i) *A. oryzae* transformant expressing the empty vectors; (ii) authentic **7**; (iii) *A. oryzae* transformant expressing the *staA*, *staB*, and *staC* genes; (iv) *A. oryzae* transformant expressing *staABC* and *staD*. (C) HPLC analysis of metabolites from (i) wild-type *S. chartarum* and (ii) the Δ*staD* strain. (D) HPLC analysis of *in vitro* enzymatic reactions: (i) **4** with StaD; (ii) **4** with inactivated StaD. (E) Schematic representation of the oxidation of **4** by StaD.

as candidates and individually expressed in *A. oryzae*−*staABC*. The accumulated metabolites in each of transformants were analyzed by HPLC−MS, which revealed that **7** was detected as a product only in *A. oryzae-staABC* + *A01136* (Fig. 4B), indicating that A01136 (StaD) could convert **4** to **7**. Deletion of *staD*, leading to the complete abolition of **2** and accumulation of precursor **4** (Fig. 4C, ii), further confirmed the involvement of the candidate gene *staD* in the biosynthesis of **2**.

Furthermore, the activity of StaD toward **4** *in vitro* was investigated. The intronless *staD* gene and *Arabidopsis thaliana* cytochrome P450 reductase (CPR) gene (*ATR1*, a general CPR gene), which functions as a redox partner[47], were cloned and inserted into the pESC-His and pESC-Leu expression vectors, respectively, and subsequently co-transformed into the INVSc1 yeast strain. LC−MS analysis revealed that incubation of the microsomal enzyme StaD/ATR1 with **4** in the presence of NADPH resulted in the production of **7** (Fig. 4D and E). Overall, StaD has been functionally characterized as an oxygenase that catalyzes the oxidation of 8′-methyl in **4** to a hydroxymethyl in the biosynthesis of **2**.

2.4. *Short-chain dehydrogenases/reductases staG, H, and H′ catalyze 3-OH epimerization*

Intriguingly, naturally occurring phenylspirodrimane meroterpenoids generally exhibit a 3α-OH configuration, with the exceptions being L-671,776 (**11**)[43,44], factor A[43,44], chartarlactam G[48], and chartarlactam I[48], which are characterized by 3β-OH attachment. As mentioned above, L-671,776 (**11**) is an intermediate of **2**. Therefore, it is suggested that there are additional enzyme(s) for the epimerization of 3β-OH to 3α-OH in **2**, probably through oxidation to a ketone followed by stereo-selective reduction to an alcohol with short-chain dehydrogenases/reductases (SDRs)[49-51].

Due to the presence of two SDRs around the *sta-1* cluster and one nearby *sta-2* cluster, we deleted the three SDRs (Fig. S4). Whereas, all the knockout strains still retained the ability to produce **2**, which suggested that the corresponding SDR genes were outside of the *sta-1* and *sta-2* clusters. Thus, hierarchical clustering analysis based on the differential transcriptomes was also employed to mine the gene(s) involved in **2** biosynthesis from the SDRs. As a result, we selected 27 SDR genes (excluding the three SDRs around the gene clusters) that exhibited similar expression profiles to those of *staA*−*F* (Supporting Information Fig. S14). Next, based on an expression correlation analysis using *staD* as bait, 9 of 27 SDR genes ($r > 0.6$) were selected for functional characterization (Fig. S14). To identify the specific SDRs involved in **2** biosynthesis, 9 mutants in which each gene was inactivated individually were generated. Compared with that of the wild-type strain, the metabolic profile of Δ*A00251* (Δ*staG*) showed complete elimination of **2** and a 90% decrease in yield of **3** (Fig. 5A). Additionally, intermediate (**11**) was the predominant

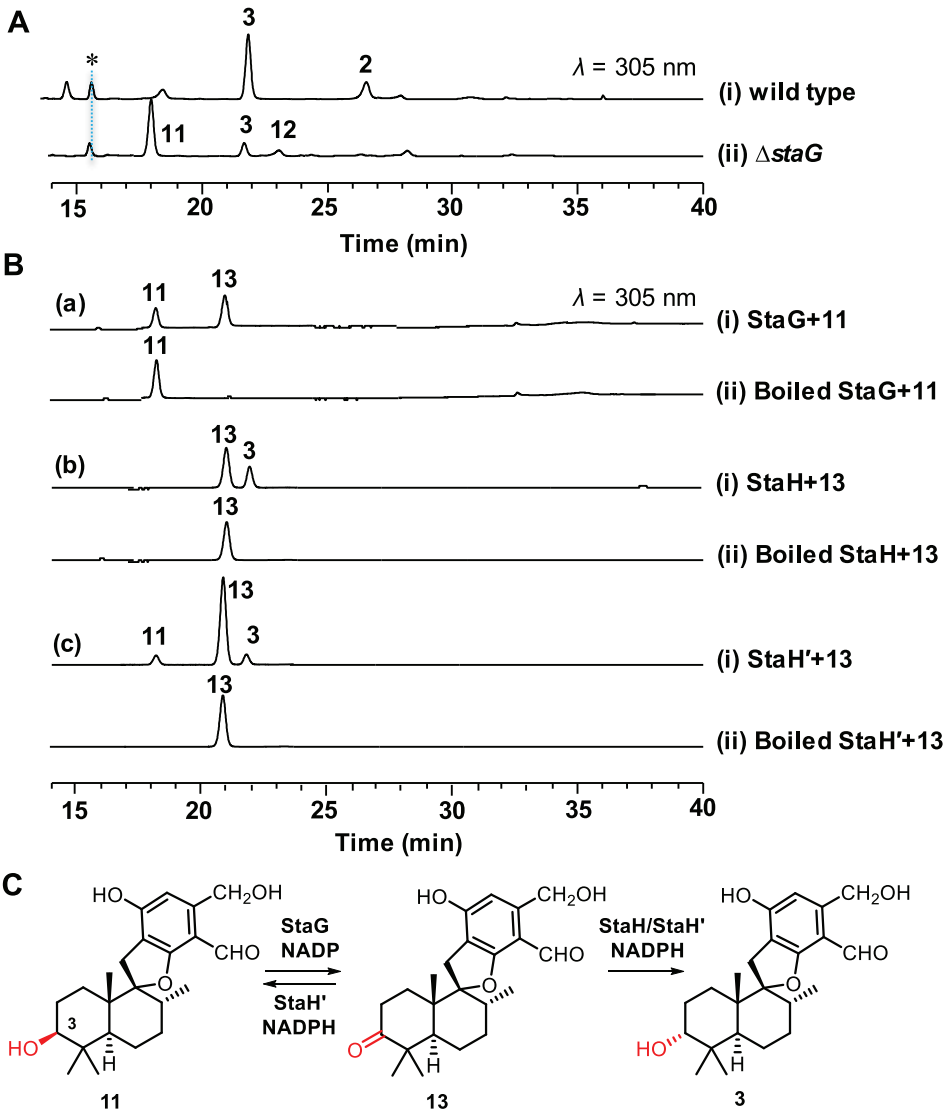

Figure 5 Functional characterizations of StaG, StaH, and StaH'. (A) HPLC analysis of metabolites from wild-type *S. chartarum* and the Δ*staG* strain: (i) wild-type; (ii) the Δ*staG* strain. (B) Biochemical functions of StaG, StaH, and StaH' *in vitro*. (a) HPLC analysis of *in vitro* enzymatic reactions: (i) **11** with StaG; (ii) **11** with inactivated StaG. (b) HPLC analysis of *in vitro* enzymatic reactions: (i) **13** with StaH; (ii) **13** with inactivated StaH. (c) HPLC analysis of *in vitro* enzymatic reactions: (i) **13** with StaH'; (ii) **13** with inactivated StaH'. (C) Schematic representation of the epimerization of 3-OH in **11** by StaG, StaH and StaH'. The asterisk (*) denotes the unrelated metabolite mellein.

product, along with another product, **12** (Fig. 5A). To elucidate the structures of these two products, scale-up (8 L) fermentation of this mutant was performed, **11** and **12** were isolated and identified as L-671,776 (**11**) and factor A (**12**)[43,44], respectively, based on MS and NMR analyses (Table S5 and Fig. S7; Fig. 2B). Compound **12** was a C-3 stereoisomer of **2**, and the 3β-OH stereochemistry of **12** was readily established through the coupling patterns of H-3 (dd, J = 10.5 and 5.5 Hz in **12** *vs.* brs in **2**) and the chemical shift of C-3 (76.4 in **12** *vs.* 75.3 in **2**). These data indicated that StaG was involved in the epimerization of 3-OH in the biosynthesis of **2**.

To investigate the function of StaG, the coding region of *staG* was cloned and inserted into the pET-28a expression vector and subsequently expressed at a high-level in *E. coli* Transetta (DE3) (Fig. S9). When **11** was incubated with StaG in the presence of NADP, a new peak was detected (Fig. 5B, a), which was isolated and structurally identified as 3-oxo-mer-NF5003E (**13**) by NMR and MS analyses (Table S5 and Fig. S7; Fig. 5C). Thus, StaG is the SDR that oxidizes the 3β-OH of **11** to generate the corresponding ketone (**13**) in **2** biosynthesis.

Given the 3α-OH in **2**, it is postulated that there was at least one SDR for the stereo-selective reduction of 3-carbonyl in **13** to 3α-OH. The remaining 18 of the 27 SDR genes were cloned from *S. chartarum* cDNA and individually expressed in *E. coli*. After purification by Ni-affinity chromatography, each of the recombinant enzymes was biochemically assayed with **13** as the substrate in the presence of NADPH. LC–MS analysis of the reactions revealed that two functionally redundant SDRs, StaH (A00109) and StaH' (A07268), could reduce **13** to **3** (Fig. 5B, b and c). Furthermore, an additional product, **11**, was observed in an *in vitro* assay of StaH' (Fig. 5B and c), indicating the non-stereoselectivity of StaH' toward **13**.

Next, Δ*staH* and Δ*staH′* mutant strains were individually generated (Fig. S2), LC−MS analysis of the metabolites revealed that both mutants were able to produce **2** in almost equal amounts compared to the wild-type strain, confirming their functional redundancy (Fig. S6, iii and iv). Then, a Δ*staH*/Δ*staH′* double mutant strain was constructed (Fig. S2), however, **2** at a comparable yield to that of the wild-type strain was detected by HPLC analysis (Fig. S6 and v). These results suggested the existence of additional enzymes except for StaH and StaH' in *S. chartarum* for the conversion of **13** to **2**. In addition, all the previously mentioned SDR knockout genes (8 genes with an expression correlation of $r > 0.6$ and 3 genes around clusters) were subjected to biochemical characterization *in vitro*, however, no enzyme could convert **13** to **3** (data not shown). Compound **11** with 3β-OH configuration was not detected by HPLC−MS analysis in the wild-type strain, which might be attributed to the high-reactivity StaG and stereoselective reduction by StaH (Fig. 5C), together with the presence of other unidentified enzymes for specific reduction of 3-carbonyl to 3α-OH.

2.5. *FAD-dependent oxidases staI/I′ catalyze C8′ oxidation*

Structurally, it is evident that further oxidation of the C-8′ hydroxymethyl group in **3** is necessary to form an aldehyde in the biosynthesis of **2**, possibly by FAD-dependent oxidases[52,53], cytochrome P450s[46], and alcohol dehydrogenases[54]. Based on the catalyzed property of reported enzymes[52,53] with the ability to convert benzyl alcohol to benzaldehyde, we first focused on FAD-dependent oxidase. Due to the non-clustered nature of the genes involved in the biosynthesis of **2** in *S. chartarum*, hierarchical clustering and expression correlation analyses of all the FAD-dependent oxidase genes with the identified biosynthetic genes (*staA*−*G*) were also performed. Consequently, 16 candidate genes exhibiting similar expression profiles and relatively high expression correlations ($r > 0.6$, *staD* as bait) were selected for cloning and heterologous expression in *E. coli* (Supporting Information Fig. S15). No product was detected in any of the assays in which each of these recombinant enzymes was incubated with **3** in the presence of FAD. Whereas, **3** was consumed by 90% when incubated with the two enzymes encoded by *A09469* (*staI*) and *A04828* (*staI′*) compared with the control group (Fig. 6A, iii and iv). We reasoned that StaI and StaI' might oxidize C-8′ hydroxymethyl to an aryl aldehyde, leading to the formation of a product bearing a reactive *O*-phthalaldehyde unit. As mentioned previously, the *O*-phthalaldehyde unit can react with the free NH_2 group[27,42] of amino acid residues in proteins and yield undetectable complex products. It is suggested that an exogenous amino acid with a free NH_2 group during incubation could be used as a "competitor" for capturing by general LC−MS analysis. Therefore, incubations with purified StaI or StaI', **3**, FAD, and two $-NH_2$-containing L-lysine, were performed. As expected, the conversion of **3** to **1** was clearly detected by LC−MS (Fig. 6A, v and vi). Similarly, upon conducting the assay with the addition of L-phenylalanine, the corresponding product **15** was also observed (Supporting Information Fig. S16A). The structures of **1** and **15** were confirmed by comparing their HPLC retention times, UV, and MS spectra with those of authentic standards (Fig. 6A and Fig. S16A and Fig. S7). These observations also demonstrated that the nonenzymatic reaction between free amino acids and the *O*-phthalaldehyde product accomplishes the synthesis of both **1** and **15** (Fig. 6B and Fig. S16B).

The above results indicated that both StaI and StaI' were responsible for converting 8′-hydroxymethyl to 8′-aldehyde. Whereas both the Δ*staI* and *ΔstaI′* mutant strains (Fig. S2) still retained the ability to produce **2** (Fig. S6, vi and vii), confirming their functional redundancy. In addition, the double inactivated Δ*staI*/*ΔstaI′* could produce **2**, albeit in a lower yield (Fig. S6, viii), suggesting the presence of other enzyme(s) for the reaction in this strain.

2.6. *Multiple pathways in the biosynthesis of 2*

Considering the generation and structural characteristics of **8**, **10a**, and **12** (Fig. 2B) in the mutants mentioned above, together with the results of the feeding experiment (Fig. S8), we presumed that **8**, **10**, and **12** are on-pathway biosynthetic intermediates and that the oxidation of C-8′ from a hydroxymethyl group to an aldehyde may also occur prior to the epoxidation of the prenyl group. Therefore, individual incubation of **7** and FAD with recombinant StaI and StaI' was performed, respectively, and decreases of more than 50% were observed for **7** (Supporting Information Fig. S17). These results indicated that StaI and StaI' could not only transform phenylspirodrimane **3** into **2** but also convert linear precursor **7** into **8**. Additionally, **11** and **13** can also be converted to the corresponding *O*-phthalaldehyde products **12** and **14** by StaI and StaI', respectively (Supporting Information Figs. S18 and S19). The linear precursor **7** also can be further modified by StaE to yield **9** (Fig. 2B, pink arrow, pathway a) or sequentially modified by StaI/I′ and StaE to produce **10** (Fig. 2B, blue arrow, pathway b). Subsequently, **3** and **2** can be generated from **9** and **10** by the sequential catalysis of StaF, G, and H/H′, and **3** can be converted to **2** by StaI/I′. Moreover, intermediates such as compounds **9**, **11**, and **13** can enter pathway b through conversion mediated by StaI/I′ (Fig. 2B). Taken together, these observations suggested that the biosynthesis of **2** involved multiple pathways rather than a strictly linear route (Fig. 2B).

Subsequently, the kinetic parameters of StaE, StaI and StaI' were calculated using linear substrate **7** and phenylspirodrimane substrate **3**, respectively (Supporting Information Fig. S20). StaE, StaI, and StaI' exhibited K_m values of 135.0, 816.7, and 501.3 μmol/L for **7**, respectively. The k_{cat}/K_m value of StaE for **7** was 1170 L/mol·s, which was 900- and 190-fold higher than those corresponding values of StaI and StaI' (1.22 and 5.98 L/mol·s, respectively). Meanwhile, StaI and StaI' exhibited higher catalytic efficiencies when utilizing substrate **3** (168.15 and 39.03 L/mol·s, respectively) compared to substrate **7**. Cumulatively, these findings indicate that intermediate **7** is more easily catalyzed by StaE than StaI and StaI', and oxidation of C-8′ occurs at a later stage in the biosynthetic pathway. Based on the current results, pathway a appears to be the predominant route, however, the significance of pathway b cannot be overlooked due to the potential presence of functionally redundant enzymes beyond StaI/I′, which have yet to be fully characterized. Furthermore, prenylated isoindolinone derivatives originating from intermediate **8** (*via* pathway b) have been isolated in this wild-type strain[55], providing additional evidence for the existence of pathway b. Even more, the biosynthetic pathway is probably more complex than the proposed routes in Fig. 2B.

Generally, the biosynthetic genes for natural products in fungi are clustered, and the corresponding enzymes usually exhibit substrate and reaction specificity. In this work, we observed that those biosynthetic genes for **2** were scattered across seven distinct regions in the genome, and some corresponding enzymes (*e.g.*, StaE−I, H′, and I′) showed substrate promiscuity. Also, multiple

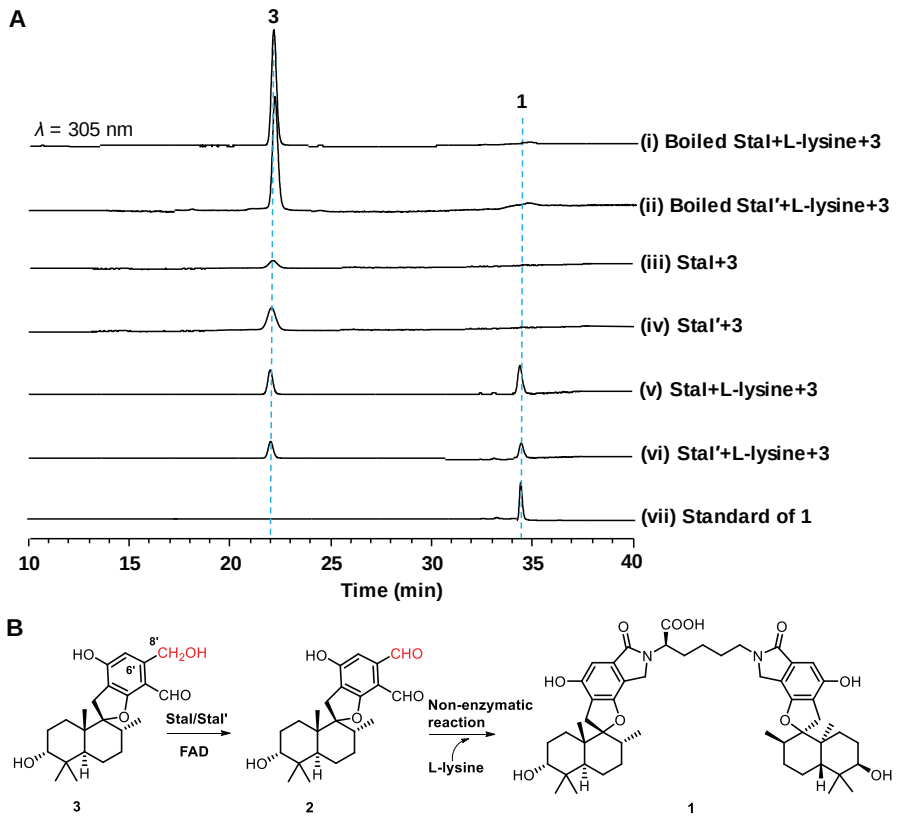

Figure 6 Biochemical function of StaI and StaI' *in vitro*. (A) HPLC analysis of *in vitro* enzymatic reactions with StaI and StaI': (i) **3** and L-lysine with inactivated StaI; (ii) **3** and L-lysine with inactivated StaI'; (iii) **3** with StaI; (iv) **3** with StaI'; (v) **3** and L-lysine with StaI; (vi) **3** and L-lysine with StaI'; (vii) authentic **1**. (B) Schematic representation of the oxidation of **3** by StaI and StaI'.

enzymes for one reaction were observed. These might be the reasons why the biosynthesis of **2** displays a complex network and the fact that **2** can still be produced when the functionally verified genes are deleted. Furthermore, some studies have also reported that metabolic networks have evolved to minimize the disruption of key metabolic pathways through the establishment of redundant genes/reactions[56,57]. Consequently, we hypothesize that the functional redundancy and the presence of multiple pathways in this fungus may be attributed to both metabolic flexibility and evolutionary pressures.

Collectively, the biosynthesis of **2**, involves two clusters (*sta-1* and *sta-2*) and another five dispersed genes, was elucidated by genome mining and transcriptome-based hierarchical clustering and expression correlation analyses. To our knowledge, this is first report on multilocus genes away from cluster in the biosynthesis of fungal natural products. Considering that the genus *Stachybotrys* has the capacity to produce a diverse array of phenylspirodrimanes derived from **2**[15,18-26], it is likely that there exist the corresponding biosynthetic genes within this genus. To verify this speculation, we conducted a homology analysis of the biosynthetic genes associated with **2** in publicly available genome sequences of the *Stachybotrys* genus. Genome mining revealed the homologues are also scattered across multiple loci in *S. chartarum* IBT 7711, *S. chlorohalonata* IBT 40285, and *S. elegans*, respectively. Therefore, genes for phenylspirodrimane meroterpenoid biosynthesis are generally unclustered in the genomes of *Stachybotrys* genus.

2.7. *Bioactivities of intermediates in the biosynthesis of* **2**

It has been reported that **1** exhibit strong inhibitory activity toward inactivation of the $hNa_V1.2$ channels (IC_{50} = 0.22 μmol/L)[27]. To identify $hNa_V1.2$ channels inhibitors with increased potency and selectivity, we tested all the isolated compounds from the process of elucidation of **2** biosynthesis. The results indicated that intermediates **6**–**8**, and **9a** exhibited significant inhibitory effects on the inactivated state of $hNa_V1.2$ channels with IC_{50} values of 0.15, 0.04, 0.28, and 1.91 μmol/L, respectively (Table 1 and Supporting Information Fig. S21), and among them intermediates **6** and **7** showed stronger inhibitory activity than **1**. Analyzing the structure-activity relationship revealed that intermediates containing a farnesyl side chain exhibited significantly stronger inhibitory activity compared to those with a phenylspirodrimane skeleton, especially when there is no modification on the side chain. Additionally, the presence of aldehyde and hydroxymethyl groups in the polyketide-derived portion is beneficial for inhibitory activity. What's more, the inhibition effects of these compounds on the inactivated state were higher than those on the resting state, with significantly higher activity than the marketed sodium channel-targeting antiepileptic drug carbamazepine (Table 1), suggesting their potential for new antiepilepsy agents. Whereas the bioactive **6** and **7** only can be isolated from Δ*staB* and 2-day-old Δ*sta*E mutant with low yield (7.3 and 0.9 mg/L), respectively. Based on

Table 1 Inhibition and state selectivity of compounds **6**−**8**, and **9a** on $hNa_V1.2$ channels.[a]

Compd	Resting state		Inactivated state	
	Inhibition (%)	IC_{50} (μmol/L)	Inhibition (%)	IC_{50} (μmol/L)
6	97.7 ± 2.3	1.61 ± 0.13	100	0.15 ± 0.01
7	97.3 ± 2.6	2.32 ± 0.01	100	0.044 ± 0.01
8	89.2 ± 10.6	2.57 ± 0.003	100	0.28 ± 0.02
9a	22.1 ± 10.9	31.97 ± 0.03	73.3 ± 17.2	1.91 ± 0.04
Carbamazepine[b]	0.9 ± 0.8	>300	17.6 ± 5.6	60.01 ± 6.11

[a]The inhibitory rates were obtained with compounds at 10 μmol/L. Experiments were performed in triplicate.
[b]Positive control.

the above biosynthesis knowledge of **2**, the *A. oryzae* transformants harboring *staAC* and *staABCD* were individually constructed to produce **6** and **7** with yield 108.7 mg/L and 13.8 mg/L, respectively. These findings provide a source of bioactive compounds for antiepileptic drug discovery.

3. Conclusions

In summary, we herein first elucidated the complete biosynthetic pathway of the phenylspirodrimane meroterpenoid stachybotrydial (**2**) in *S. chartarum* by genome mining, gene inactivation, heterologous expression, and biochemical experiments with the aid of hierarchical clustering and expression correlation analyses. The biosynthetic genes for **2** are not well-defined gene clusters, but exhibit unusual discreteness involving two gene clusters (*sta-1* and *sta-2*, six genes) and five genes located apart from the two clusters. Moreover, the biosynthetic pathways of **2** involve multiple routes rather than a strictly linear one, highlighting their potential for diverse and intricate chemical transformations. In addition, four biosynthetic intermediates exhibited significant antiepileptic activity, and the yields of two most bioactive compounds were greatly increased by heterologous expression. The complete elucidation of the biosynthesis of **2** in this work can offer an opportunity for engineered microorganisms to produce bioactive dimer **1** and other compounds for drug discovery, also provide new insights into the intricate biosynthesis of fungal natural products. Furthermore, these findings provide important knowledge toward the biosynthesis and structural diversity of meroterpenoids and shed light on transcriptome-based hierarchical clustering and expression correlation analyses are powerful strategies to discover and identify the multilocus and unclustered biosynthetic genes in fungi.

4. Experimental

4.1. Strains and culture conditions

The wild-type strain *S. chartarum* CGMCC 3.5365 was obtained and cultured as described previously[23-26]. *E. coli* DH5α was used for routine cloning and plasmid extraction, *E. coli* Transetta (DE3) and BL21 (TransGen Biotech, China) were used for protein expression. The heterologous expression host *Aspergillus oryzae* NSAR1 was kindly gifted by Prof. Ikuro Abe and Prof. Katsuhiko Kitamoto at The University of Tokyo and Prof. Katsuya Gomi at Tohoku University. *Saccharomyces cerevisiae* INVSc1 was used for terpene cyclase and cytochrome P450 expression. Additional detailed methods of strains culture were shown in Supporting Information

4.2. Construction of co-expression system of staABC, staABCD, staE, and staEF

For the construction of fungal expression plasmids for *staA*, *B*, *C*, *E*, and F, the genes were amplified from *S. chartarum* genomic DNA with the primers listed in Supporting Information Table S7. Additional detailed construction methods were shown in Supporting Information

4.3. Transformation of A. oryzae NSAR1

Transformation of *A. oryzae* NSAR1 were performed by the protoplast−polyethylene glycol method[16,40]. Additional detailed methods were shown in Supporting Information

4.4. Construction of deletion cassette

The knockout cassettes were constructed by homologous recombination method. For creation of *staB*−*I*, *H*′, and *I*′ deletion strains, approximately 1.5 kbp sequences located upstream and downstream the target genes were amplified from genomic DNA of *S. chartarum* CGMCC 3.5365 using primer pairs in Table S7. Polymerase chain reactions were performed using high-fidelity FastPfu Fly DNA polymerase (TransGen Biotech, China). Additional detailed construction methods were shown in Supporting Information

4.5. Transformation of S. chartarum

Transformation of *S. chartarum* were performed by the protoplast−polyethylene glycol method. Additional detailed methods were shown in Supporting Information

4.6. Expression and purification of recombination proteins

pCold-TF-StaE, pET28a-StaG, pET28a-StaH, and pET28a-StaH′ were used to transform *E. coli* Transetta (DE3) and pCold-TF-StaI was used to transform *E. coli* BL21 for His_6-tagged protein induction and purification. For expression of *staI*′, the first 16 amino acid residues (putative N-terminal signal sequence) of the protein were excluded. Then the pET-SUMO-StaI′ was transformed into *E. coli* Transetta (DE3) cells for His_6-tagged protein induction and purification. Additional detailed methods of protein expression and purification were shown in Supporting Information

4.7. Expression of StaC, StaD, and StaF in yeast

The coding regions of StaC, StaD, StaF, and ATR1 (a cytochrome P450 reductase from *Arabidopsis thaliana*) were individually cloned into a yeast expression vector, pESC, under the control of the GAL10 yeast promoter to yield pESC-His-StaC, pESC-His-StaD, pESC-His-StaF, and pESC-Leu-ATR1. After verification of the sequence, the plasmids pESC-His-StaD and pESC-Leu-ATR1 were co-introduced into *Saccharomyces cerevisiae* INVSc1 strain for expression. The plasmids of pESC-His-StaC and pESC-His-StaF were transformed to INVSc1 strain for expression analysis, respectively. Additional detailed methods were shown in Supporting Information

4.8. In vitro biochemical assays

All the reactions were carried out in 1.5 mL Eppendorf tubes at 30 °C for 12 h. The reaction was terminated by the addition of 200 μL methanol. Protein precipitate was removed by centrifugation (15,000×*g*, 40 min) (Sigma, 3K15, Germany). Then the reaction mixture were used for LC−MS analysis and three parallel assays were routinely carried out. HPLC analyses were performed as described in Supporting Information

4.9. Feeding experiments

The mycelia of *A. oryzae* transformants harboring *staE* and *staEF* were inoculated in 50 mL DPY medium in 250 mL Erlenmeyer flasks at 28 °C, 150 rpm (Taicang Haocheng, HZQ-F100, Taicang, China). Substrates (**7**) was dissolved in dimethyl sulfoxide (DMSO) at a concentration of 10 mg/mL. After culture 2 days, the cells were transferred into CD medium to induce, then 100 μL of **7** was added to the culture of *A. oryzae*-staE *and A. oryzae*-staEF, respectively, and culture at 28 °C, 180 rpm (Taicang Haocheng) for 24 h. Then, the culture was extracted with ethyl acetate and concentrated *in vacuo*. The extracts were analyzed by LC−MS.

The Δ*staB* mutant cells were cultured in a 50 mL scale at 28 °C and 150 rpm (Taicang Haocheng) in PDB medium. After 48 h cultivation, compounds **7** and **8** (1.0 mg, 20 mmol/L) dissolved in DMSO were individually supplemented into the cultures and cultured for another 12 h. The metabolic extract was analyzed by LC−MS.

4.10. Scale-ups of enzymatic reaction

To obtain sufficient amounts of **9a**, **11**, and **13** for structural characterization, the scale-ups of enzymatic reaction were performed. Additional detailed processes were shown in Supporting Information

4.11. Analysis and isolation of metabolites

For small scale analysis, *S. chartarum* wild type and its mutant strains (Δ*staB*, *C*, *D*, *E*, *F*, *G*, *H*, *H′*, *H/H′*, *I*, *I′*, and *I/I′*) were cultivated in Erlenmeyer flasks (250 mL) containing 100 mL of PDB medium on a shaker at 150 rpm (Taicang Haocheng), 28 °C for 7 days. The cultures were extracted with the same volume of ethyl acetate (EtOAc) twice and evaporated to dryness. The dried extract was dissolved in methanol and analyzed by LC−MS. For isolation of metabolites, extract was subjected to the column chromatography and further purification by semi-preparative HPLC. Additional detailed methods were shown in Supporting Information

4.12. $hNa_V1.2$ channels inhibitory activity assay

The $hNa_V1.2$ channels inhibitory experments were carried out as described previously[27]. Additional detailed methods were shown in Supporting Information

Acknowledgments

This work was financially supported by National Key R&D Program of China (2024YFA0919900), National Natural Science Foundation of China (No. 81803403), and CAMS Innovation Fund for Medical Sciences (CIFMS, No. 2021-I2M-1-029, China). We are grateful to Prof. Ikuro Abe and Prof. Katsuhiko Kitamoto at The University of Tokyo and Prof. Katsuya Gomi at Tohoku University for kindly gifting the expression host *A. oryzae* NSAR1 strain and vectors.

Author contributions

Jimei Liu performed the biochemical and genetic experiments; Yaotian Han and Songyang Sui isolated some intermediates; Yangyang Duan, Min Zhang, and Keping Feng established the genetic manipulation system; Jun Wu and Haibo Yu performed the biological activity experiments; Dawei Chen and Jungui Dai made the research planning and supervision; Jimei Liu, Ridao Chen, Kebo Xie, Dawei Chen and Jungui Dai wrote the manuscript. All the authors approved the final manuscript.

Conflicts of interest

The authors declare no conflicts of interest.

Data availability

*S. chartaru*m RNA-seq and DNA-seq data associated with this article have been deposited into the NCBI Sequence Read Archive with BioProject identifiers PRJNA1142863 and PRJNA1143151, respectively. The gene sequences of StaA-I, H′, and I′ of *S. chartarum* are deposited in GenBank as accession Nos PP948689−PP948699. Additional detailed experimental procedures, description on the isolation of compounds, supplementary tables and figures, NMR and HRESIMS spectra (Supporting Information Fig. S22−S63).

Appendix A. Supporting information

Supporting information to this article can be found online at https://doi.org/10.1016/j.apsb.2025.09.015.

References

1. Geris R, Simpson TJ. Meroterpenoids produced by fungi. *Nat Prod Rep* 2009;**26**:1063−94.
2. Matsuda Y, Abe I. Biosynthesis of fungal meroterpenoids. *Nat Prod Rep* 2016;**33**:26−53.
3. Matsuda Y, Abe I. *Fungal meroterpenoids. Comprehensive natural products III: chemistry and biology.* Elsevier; 2020. p. 445−78.

4. Barra L, Abe I. Chemistry of fungal meroterpenoid cyclases. *Nat Prod Rep* 2021;**38**:566−85.
5. Matsuda Y, Awakawa T, Abe I. Reconstituted biosynthesis of fungal meroterpenoid andrastin A. *Tetrahedron* 2013;**69**:8199−204.
6. Matsuda Y, Awakawa T, Wakimoto T, Abe I. Spiro-ring formation is catalyzed by a multifunctional dioxygenase in austinol biosynthesis. *J Am Chem Soc* 2013;**135**:10962−5.
7. Lo HC, Entwistle R, Guo CJ, Ahuja M, Szewczyk E, Hung JH, et al. Two separate gene clusters encode the biosynthetic pathway for the meroterpenoids austinol and dehydroaustinol in *Aspergillus nidulans*. *J Am Chem Soc* 2012;**134**:4709−20.
8. Matsuda Y, Iwabuchi T, Wakimoto T, Awakawa T, Abe I. Uncovering the unusual D-ring construction in terretonin biosynthesis by collaboration of a multifunctional cytochrome P450 and a unique isomerase. *J Am Chem Soc* 2015;**137**:3393−401.
9. Zhang T, Wan J, Zhan Z, Bai J, Liu B, Hu Y. Activation of an unconventional meroterpenoid gene cluster in *Neosartorya glabra* leads to the production of new berkeleyacetals. *Acta Pharm Sin B* 2018;**8**: 478−87.
10. Matsuda Y, Wakimoto T, Mori T, Awakawa T, Abe I. Complete biosynthetic pathway of anditomin: nature's sophisticated synthetic route to a complex fungal meroterpenoid. *J Am Chem Soc* 2014;**136**: 15326−36.
11. Matsuda Y, Bai T, Phippen CB, Nødvig CS, Kjærbølling I, Vesth TC, et al. Novofumigatonin biosynthesis involves a non-heme iron-dependent endoperoxide isomerase for orthoester formation. *Nat Commun* 2018;**9**:2587.
12. Ellestad G, Evans Jr R, Kunstmann M. Some new terpenoid metabolites from an unidentified *Fusarium* species. *Tetrahedron* 1969;**25**: 1323−34.
13. Tamura G, Suzuki S, Takatsuki A, Ando K, Arima K. Ascochlorin, a new antibiotic, found by paper-disc agar-diffusion method. I. isolation, biological and chemical properties of ascochlorin. *J Antibiot* 1968;**21**: 539−44.
14. Sasaki H, Hosokawa T, Sawada M, Ando K. Isolation and structure of ascofuranone and ascofranol, antibiotics with hypolipidemic activity. *J Antibiot* 1973;**26**:676−80.
15. Wang A, Xu Y, Gao Y, Huang Q, Luo X, An H, et al. Chemical and bioactive diversities of the genera *Stachybotrys* and *Memnoniella* secondary metabolites. *Phytochem Rev* 2015;**14**:623−55.
16. Li C, Matsuda Y, Gao H, Hu D, Yao XS, Abe I. Biosynthesis of LL-Z1272β: discovery of a new member of NRPS-like enzymes for aryl-aldehyde formation. *Chembiochem* 2016;**17**:904−7.
17. Araki Y, Awakawa T, Matsuzaki M, Chod R, Matsuda Y, Hoshino S, et al. Complete biosynthetic pathways of ascofuranone and ascochlorin in *Acremonium egyptiacum*. *Proc Natl Acad Sci USA* 2019; **116**:8269−74.
18. Kaise H, Shinohara M, Miyazaki W, Izawa T, Nakano Y, Sugawara M, et al. Structure of K-76, a complement inhibitor produced by *Stachybotrys complementi* nov. sp. K-76. *J Chem Soc Chem Commun* 1979;**16**:726−7.
19. Wu B, Oseker V, Wiese J, Malien S, Schmaljohann R, Imhoff JFS. Spirocyclic drimanes from the marine fungus *Stachybotrys* sp. strain MF347. *Mar Drugs* 2014;**12**:1924−38.
20. Zhang P, Li Y, Jia C, Lang J, Niaz SI, Li J, et al. Antiviral and anti-inflammatory meroterpenoids stachybonoids A−F from the crinoid-derived fungus *Stachybotrys chartarum* 952. *RSC Adv* 2017;**7**: 49910−6.
21. Zhang H, Yang MH, Zhuo FF, Gao N, Cheng XB, Wang XB, et al. Seven new cytotoxic phenylspirodrimane derivatives from the endophytic fungus *Stachybotrys chartarum*. *RSC Adv* 2019;**9**: 3520−31.
22. Kim JW, Ko SK, Kim HM, Kim GH, Son S, Kim GS, et al. Stachybotrysin, an osteoclast differentiation inhibitor from the marine-derived fungus *Stachybotrys* sp. KCB13F013. *J Nat Prod* 2016;**79**: 2703−8.
23. Zhao J, Feng J, Tan Z, Liu J, Zhao J, Chen R, et al. Stachybotrysins A−G, phenylspirodrimane derivatives from the fungus *Stachybotrys chartarum*. *J Nat Prod* 2017;**80**:1819−26.
24. Zhao J, Feng J, Tan Z, Liu J, Zhang M, Chen R, et al. Bistachybotrysins A−C, three phenylspirodrimane dimers with cytotoxicity from *Stachybotrys chartarum*. *Bioorg Med Chem Lett* 2018;**28**:355−9.
25. Zhang M, Feng J, Jia X, Zhao J, Liu J, Chen R, et al. Bistachybotrysins D and E, one stereoisomeric pair of cytotoxic phenylspirodrimane dimers from *Stachybotrys chartarum*. *Chin Chem Lett* 2019;**30**:435−8.
26. Liu J, Jia X, Zhao J, Feng J, Chen M, Chen R, et al. Bistachybotrysins L−V, bioactive phenylspirodrimane dimers from the fungus *Stachybotrys chartarum*. *Org Chem Front* 2020;**7**:531−42.
27. Liu J, Wang Z, Wu J, Han Y, Ye F, Zhang T, et al. Structural diversification of phenylspirodrimane lactams by employing a biosynthetic intermediate. *Chin Chem Lett* 2023;**34**:108363.
28. Deng WP, Zhong M, Guo XC, Kende AS. Total synthesis and structure revision of *Stachybotrys* spirolactams. *J Org Chem* 2003;**68**:7422−7.
29. Cano MJ, Bouanou H, Tapia R, Alvarez E, Alvarez-Manzaneda R, Chahboun R, et al. NIS−PPh3: a selective reagent for the spiroannulation of o-allyl phenols. Total synthesis of corallidictyal D. *J Org Chem* 2013;**78**:9196−204.
30. Tao H, Abe I. Enzymology and biosynthesis of the orsellinic acid derived medicinal meroterpenoids. *Curr Opin Biotechnol* 2021;**69**: 52−9.
31. Owen JG, Reddy BVB, Ternei MA, Charlop-Powers Z, Calle PY, Kim JH, et al. Mapping gene clusters within arrayed metagenomic libraries to expand the structural diversity of biomedically relevant natural products. *Proc Natl Acad Sci U S A* 2013;**110**: 11797−802.
32. Yamanaka K, Reynolds KA, Kersten RD, Ryan KS, Gonzalez DJ, Nizet V, et al. Direct cloning and refactoring of a silent lipopeptide biosynthetic gene cluster yields the antibiotic taromycin A. *Proc Natl Acad Sci USA* 2014;**110**:1957−62.
33. Keller NP, Turner G, Bennett JW. Fungal secondary metabolism from biochemistry to genomics. *Microbiology* 2005;**3**:937−46.
34. Zhao S, Shen Z, Zhai Z, Yin R, Xu D, Wang M, et al. Elucidation of palmarumycin spirobisnaphthalene biosynthesis reveals a set of previously unrecognized oxidases and reductases. *Angew Chem Int Ed* 2024;**63**:e202401979.
35. Sanchez JF, Entwistle R, Hung JH, Yaegashi J, Jain S, Chiang YM, et al. Genome-based deletion analysis reveals the prenyl xanthone biosynthesis pathway in *Aspergillus nidulans*. *J Am Chem Soc* 2010; **133**:4010−7.
36. Tang MC, Lin HC, Li D, Zou Y, Li J, Xu W, et al. Discovery of unclustered fungal indole diterpene biosynthetic pathways through combinatorial pathway reassembly in engineered yeast. *J Am Chem Soc* 2015;**137**:13724−7.
37. Lau W, Sattely ES. Six enzymes from mayapple that complete the biosynthetic pathway to the etoposide aglycone. *Science* 2015;**349**: 1224−8.
38. Nett RS, Lau W, Sattely ES. Discovery and engineering of colchicine alkaloid biosynthesis. *Nature* 2020;**584**:148−53.
39. Hong B, Grzech D, Caputi L, Sonawane P, López CER, Kamileen MO, et al. Biosynthesis of strychnine. *Nature* 2022;**607**:617−22.
40. Itoh T, Tokunaga K, Matsuda Y, Fujii I, Abe I, Ebizuka Y, et al. Reconstitution of a fungal meroterpenoid biosynthesis reveals the involvement of a novel family of terpene cyclases. *Nat Chem* 2010;**2**: 858−64.
41. Tang MC, Cui X, He X, Ding Z, Zhu T, Tang Y, et al. Late-stage terpene cyclization by an integral membrane cyclase in the biosynthesis of isoprenoid epoxycyclohexenone natural products. *Org Lett* 2017;**19**:5376−9.
42. Allin SM, Hodkinson CC, Taj N. Neighbouring group assistance in the formation of phthalimidines from *O*-phthalaldehyde: an "intramolecular auxiliary effect". *Synlett* 1996;**8**:781−2.

43. Falck JR, Reddy KK, Chandrasekhar S. Synthesis and structure revision of the *myo*-inositol monophosphatase inhibitor L-671,776. *Tetrahedron Lett* 1997;**38**:5245−8.
44. Stefanelli S, Sponga F, Ferrari P, Sottani C, Corti E, Brunati C, et al. Inhibitors of *myo*-inositol monophosphatase, ATCC 20928 factors A and C isolation, physico-chemical characterization and biological properties. *J Antibiot* 1996;**49**:611−6.
45. Yan D, Matsuda Y. Global genome mining-driven discovery of an unusual biosynthetic logic for fungal polyketide−terpenoid hybrids. *Chem Sci* 2024;**15**:3011−7.
46. Zhang X, Guo J, Cheng F, Li S. Cytochrome P450 enzymes in fungal natural product biosynthesis. *Nat Prod Rep* 2021;**38**:1072−99.
47. Urban P, Mignotte C, Kazmaier M, Delorme F, Pompon D. Cloning, yeast expression, and characterization of the coupling of two distantly related *Arabidopsis thaliana* NADPH-cytochrome P450 reductases with P450 CYP73A5. *J Biol Chem* 1997;**272**:19176−86.
48. Li Y, Wu C, Liu D, Proksch P, Guo P, Lin W. Chartarlactams A−P, phenylspirodrimanes from the sponge-associated fungus *Stachybotrys chartarum* with antihyperlipidemic activities. *J Nat Prod* 2014;**77**:138−47.
49. Dong LB, Zhang X, Rudolf JD, Deng MR, Kalkreuter E, Cepeda AJ, et al. Cryptic and stereospecific hydroxylation, oxidation, and reduction in platensimycin and platencin biosynthesis. *J Am Chem Soc* 2019;**141**:4043−50.
50. Matsuda Y, Awakawa T, Abe I. Reconstituted biosynthesis of fungal meroterpenoid andrastin A. *Tetrahedron* 2013;**69**:8199−204.
51. Cao Z, Li S, Lv J, Gao H, Chen G, Awakawa T, et al. Biosynthesis of clinically used antibiotic fusidic acid and identification of two short-chain dehydrogenase/reductases with converse stereoselectivity. *Acta Pharm Sin B* 2019;**9**:433−42.
52. He Y, Cox RJ. The molecular steps of citrinin biosynthesis in fungi. *Chem Sci* 2016;**7**:2119−27.
53. Nies J, Ran H, Wohlgemuth V, Yin WB, Li SM. Biosynthesis of the prenylated salicylaldehyde flavoglaucin requires temporary reduction to salicyl alcohol for decoration before reoxidation to the final product. *Org Lett* 2020;**22**:2256−60.
54. Chadha A, Padhi SK, Stella S, Venkataraman S, Saravanan T. Microbial alcohol dehydrogenases: recent developments and applications in asymmetric synthesis. *Org Biomol Chem* 2024;**22**:228−51.
55. Zhao J, Liu J, Shen Y, Tan Z, Zhang M, Chen R, et al. Stachybotrysams A−E, prenylated isoindolinone derivatives with anti-HIV activity from the fungus *Stachybotrys chartarum*. *Phytochem Lett* 2017;**20**:289−94.
56. Sambamoorthy G, Raman K. Understanding the evolution of functional redundancy in metabolic networks. *Bioinformatics* 2018;**34**:981−7.
57. Sambamoorthy G, Sinha H, Raman K. Evolutionary design principles in metabolism. *Proc R Soc A B* 2019;**286**:20190098.